Available online at www.sciencedirect.com
SCIENCE DIRECT®
Solid State Sciences 7 (2005) 905–911
Solid State Sciences
www.elsevier.com/locate/ssscie

Dielectric response in the charge-ordered $Ca_{2-x}Pr_xMnO_4$ phases

A. Castro-Couceiro [a], M. Sánchez-Andújar [a], B. Rivas-Murias [b], J. Mira [b], J. Rivas [b], M.A. Señarís-Rodríguez [a,*]

[a] *Dpto. Química Fundamental, Universidad da Coruña, 15071 A Coruña, Spain*
[b] *Dpto. Física Aplicada, Universidad de Santiago de Compostela, 15782 Santiago de Compostela, Spain*

Received 18 January 2005; received in revised form 7 March 2005; accepted 15 March 2005

Available online 14 April 2005

Abstract

We have prepared $Ca_{2-x}Pr_xMnO_4$ ($x = 0, 0.25, 0.33$ and 0.50) compounds by the so-called "liquid-mix" method. X-ray powder diffraction indicated that these compounds are single-phase materials and resistivity measurements showed that the Pr-doped samples experience charge-ordering (CO) transitions at 275 K ($x = 0.25$), 330 K ($x = 0.33$) and 315 K ($x = 0.50$). The intrinsic dielectric constants calculated by impedance spectroscopy (IS) from the values of the obtained bulk capacitances were remarkably high: 217, 37 and 80 for the $x = 0.25$, 0.33 and 0.50 samples, respectively. In addition, extrinsic factors play an important role on their dielectric response, especially at $T > 150$ K, giving rise to very high dielectric constants at room temperature ($\varepsilon'_r \sim 10^6$). Also, and for comparison, we have studied the dielectric response of Ca_2MnO_4 (non charge-ordered compound), finding much smaller dielectric constant values and an intrinsic contribution $\varepsilon'_r(\text{bulk}) = 14$, remarkably lower than in the case of Pr-doped compounds. These results could be a new evidence of the link between the charge ordered state and the increase of the dielectric constant.

Keywords: Ruddlesden–Popper manganites; Manganese oxides; Charge ordering; Dielectric response; Impedance spectroscopy

1. Introduction

In recent years, the physical properties of the manganese perovskites $Ln_{1-x}A_xMnO_3$ have been intensively investigated due to the discovery of colossal magnetoresistance (CMR) in some members of this family [1]. Numerous efforts have been done to characterize and understand this CMR effect as well as other related properties of these mixed-oxides [2]. In this context of particular interest is the study in the mixed-valence manganites of the charge-ordered state, in which the metal ions in different oxidation states order in specific lattice sites giving rise to charge localization [3]. Manganites are not the only compounds that show charge ordering; in fact, this property was first discovered in Fe_3O_4 [4] and is also present in other materials like nickelates [5], cuprates [6], etc. But the process of CO is specially interesting in the case of manganites, as it is unstable under a variety of external perturbations (including magnetic field, temperature, external and chemical pressure, X-ray and electron irradiation [7,8]) so that these systems reveal spectacular effects like metal to insulator transitions or transitions into a ferromagnetic state induced by an external magnetic field.

Other interesting properties have been recently discovered and related to the CO state, such as an enhanced dielectric response. A first evidence of a link between CO and an increase of the dielectric properties has been reported by Jardón et al. [9] and Rivadulla et al. [10] that found in $Pr_{0.67}Ca_{0.33}MnO_3$ a high capacitive behaviour that appears just below its CO temperature, $T_{CO} = 250$ K. Single-crystals of $Pr_{0.65}Ca_{0.28}Sr_{0.07}MnO_3$ [11], polycrystalline $La_{1.5}Sr_{0.5}NiO_4$ [12], $CaMn_7O_{12}$ [13,14] and polycrystalline and thin films of $La_{1-x}Ca_xMnO_3$ [15,16] also show relative high values of the dielectric constant (ε'_r around 50 or higher). In the absence of any known structural features (e.g.,

* Corresponding author. Tel.: (+34) 981167000; Fax: (+34) 981167065.
E-mail address: tonasr@udc.es (M.A. Señarís-Rodríguez).

1293-2558/$ – see front matter
doi:10.1016/j.solidstatesciences.2005.03.001

off-center atoms that are at the origin of the large dielectric response in the well-known "structural" ferroelectrics [17]) the CO state seems to play an important role in the larger value of ε'_r. Recently, theoretical studies by Efremov et al. [18] predicting a net polarization of the electric dipole moments in the CO state, also support these experimental evidences.

But many features about this behaviour remain an open question. It is therefore of interest to study the dielectric behaviour of more compounds that experience CO:

(a) To obtain more experimental data that allow confirm or rule out the link between CO and high ε'_r, and
(b) In the search for new dielectric materials with high permittivities and low loss factors, that have important applications in many electronic devices like high performance capacitors [19].

In this context, nowadays the best industrial performances are given by ferroelectrics, such as the well-known perovskite materials $BaTiO_3$, $PbTiO_3$, etc. Another oxide that has recently attracted a lot of interest is the complex perovskite compound $CaCu_3Ti_4O_{12}$ due to its room temperature frequency independent "colossal" dielectric constant [20].

In our group, and in the framework of dielectric properties of manganese oxides with CO we have focused on $Ca_{2-x}Pr_xMnO_4$ compounds, which are related to the $Pr_{0.67}Ca_{0.33}MnO_3$ perovskites, but where the dimensionality of the crystal structure has been changed from 3D to 2D. According to Ibarra et al. [21] that studied these compounds by electron microscopy, and measured their transport and magnetic properties, they exhibit a long-range charge-orbital ordering state over a wide compositional range ($0.25 \leqslant x \leqslant 0.50$) and at remarkably high temperatures ($270 \leqslant T_{CO}$ (K) $\leqslant 330$). From the magnetic point of view, these compounds are paramagnetic (PM) above 150 K and show long-range antiferromagnetic ordering of the magnetic moments of Mn^{3+} and Mn^{4+} ions below 150 K.

In this context, we have performed a detailed characterization of the dielectric properties of the Mn^{3+}/Mn^{4+} mixed oxides $Ca_{2-x}Pr_xMnO_4$ with $x = 0.25, 0.33, 0.50$, that show different CO temperatures. In order to check the influence of the CO state on their dielectric behaviour, we have also studied the dielectric properties of the Ca_2MnO_4 phase that does not show CO and where the Mn cations have a formal oxidation state of +4. Due to the controversy regarding extrinsic polarization effects as origin of giant dielectric constants [22,23] found in other ceramic materials [24,25], we have explored the influence of extrinsic factors (like grain boundary and electrode effects) by impedance spectroscopy analysis [26] and we have checked the influence of the contacts used to perform the experiments. The most outstanding results of these studies are presented in this paper.

2. Experimental

The samples were prepared by the so-called "liquid-mix" or Pechini method [27]. Pr_6O_{11} (99.9% Aldrich) was first converted into the corresponding nitrate by dissolution in diluted HNO_3 (30%). This product was then added to a 1 M citric acid aqueous solution in which stoichiometric amounts of $Mn(NO_3)_2{\cdot}5.3\ H_2O$ (98%, Aldrich) and $CaCO_3$ (>99%, Fluka) were also dissolved. After diluting the so-obtained solution, we carefully added ethyleneglycol in a proportion of 10% v/v. The resulting solution was heated at 200 °C until a brown gel was formed and whose organic matter subsequently decomposed at ~ 400 °C. The obtained ashes were given accumulative heating treatments at 600 °C/24 h and 900 °C/48 h, with intermediate grindings, and the pelletized samples were finally sintered at 1200 °C/24 h.

Room-temperature X-ray powder diffraction (XRPD) patterns of all the samples were obtained with a Siemens D-5000 diffractometer and Cu ($K\alpha$) = 1.5418 A radiation. The XRPD data were analyzed by the Rietveld profile analysis using the Rietica software [28].

The d.c. resistivity of the samples was measured by a standard four-probe technique using a homemade device.

The complex dielectric permittivity of these mangenese oxides was measured with a parallel-plate capacitor coupled to a precision LCR meter Agilent 4284 A, capable to measure in frequency range from 20 to 1 MHz. The capacitor was mounted in an aluminium box refrigerated with liquid nitrogen, and incorporating a mechanism to control the temperature up to 350 K. The samples (average size: 0.15–0.35 cm^2) were prepared to fit in the capacitor, and gold was sputtered on their surfaces to ensure good electrical contact with the electrodes. In one of the samples, additional measurements were performed using both silver paint and sputtered silver contacts. In addition, to test the optimal performance of the experimental set-up, a commercial $SrTiO_3$ sample was measured and values similar to those reported in the literature [29] were obtained.

Impedance complex plane plots were analyzed using the LEVM program [30].

3. Results and discussion

3.1. Sample characterization

Room temperature X-ray powder diffraction showed that all the samples are single phase materials with a perovskite-related K_2NiF_4 structure. In this structure, the perovskite blocks are separated one from another by the presence of rock-salt-type (Pr/Ca–O) layers along the c-axis.

Refinement of the diffraction data gave the cell parameters that are showed in Table 1. The $x = 0.25$ and 0.33 compounds were indexed on the basis of a tetragonal K_2NiF_4 structure and for the $x = 0.50$ sample, an orthorhombic cell with $a \approx b \approx a_t\sqrt{2}$ and $c = c_t$ (where a_t and c_t are the cell

Table 1
Cell parameters for the $Ca_{2-x}Pr_xMnO_4$ samples, obtained from refinements of the room temperature X-ray powder diffraction data

	a (Å)	b (Å)	c (Å)
$x = 0.00$	5.1900(1)		24.127(6)
$x = 0.25$	3.7471(1)		11.882(4)
$x = 0.33$	3.7701(5)		11.832(3)
$x = 0.50$	5.3946(3)	5.3668(3)	11.831(5)

parameters of the tetragonal K_2NiF_4 structure) was used. On the other hand, the structure of the Ca_2MnO_4 sample is related to that of the K_2NiF_4 phase, but where the MnO_6 octahedra are slightly rotated around the c-axis [31], giving rise to a tetragonal unit cell with $a \approx b \approx a_t\sqrt{2}$ and $c \approx 2c_t$. We have to note that Ibarra et al. [21] have used an orthorhombic cell ($a \approx b \approx a_t\sqrt{2}$ and $c = c_t$) to index the electron diffraction patterns of the $x = 0.25$ and $x = 0.33$ compounds. This disagreement with our results is probably due to the fact that charge ordering superstructure diffraction maxima are too weak to be observed by X-ray diffraction.

3.2. d.c. resistivity measurements

Taking into account that the resistivity is sensitive to the charge-ordering transition, d.c. resistivity of the Pr-doped samples was measured in order to estimate their CO temperature and, in general, their electrical behaviour. In Fig. 1 we show the resistivity versus temperature curves for the Pr-doped samples. As it can be seen these materials are semiconducting and their resistivity increases with doping. In addition, they all show a CO transition that gives rise to a change in slope in the logarithmic representation of resistivity versus inverse temperature (Fig. 1), where the arrows indicate the CO temperature $T_{CO} \approx 270$ K ($x = 0.25$), 330 K ($x = 0.33$) and 315 K ($x = 0.50$). These values are in good agreement with those found in the literature [21].

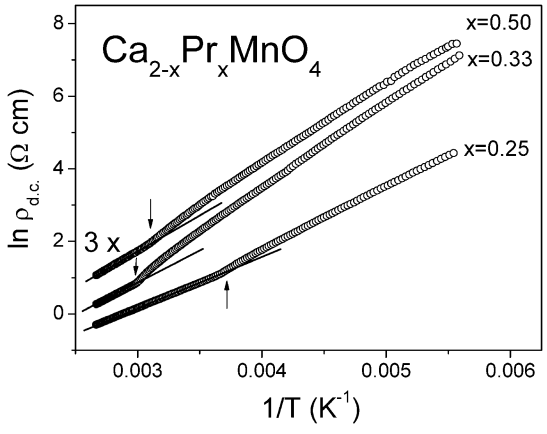

Fig. 1. Plot of logarithmic d.c. resistivity versus inverse temperature for the charge-ordered samples where the data corresponding to the $x = 0.50$ sample have been deliberately increased by a factor of 3 to make the curves more visible. The line represents the Arrhenius fit of the high temperature data and the arrows show the CO temperature.

The temperature dependence of the d.c. resistivities after and before T_{CO} follow an Arrhenius law ($\rho = Ae^{E_a/kT}$), indicating that the conduction mechanism takes place by hopping of the charge carriers. At $T > T_{CO}$ the hopping activation energy E_a, that was calculated from the corresponding linear fits, was: 119 meV, 155 meV and 172 meV for $x = 0.25$, 0.33 and 0.50, respectively. At lower temperatures (175 K $< T < T_{CO}$) higher values of E_a were obtained (148 meV, 205 meV and 192 meV, respectively).

3.3. Dielectric properties

The relative complex dielectric permittivity $\varepsilon_r = \varepsilon'_r - \varepsilon''_r$ of the samples was measured as a function of frequency and temperature.

As the results are considerably different for Pr-doped compounds compared to the Ca_2MnO_4 sample, in what follows we will separately describe these two types of behaviours. For simplicity we will first show the results for the non-charge ordered Ca_2MnO_4 material.

3.3.1. Ca_2MnO_4 (non-charge-ordered compound)

Fig. 2 shows the frequency dependence of the real part of the complex dielectric permittivity ε'_r (the so-called dielectric constant) for this sample. As it can be seen, for a given temperature the dielectric constant decreases with frequency, while for a given frequency it increases with temperature. Nevertheless, while at the lowest frequency ε_r is very strongly temperature dependent, changing from 20 ($T =$ 110 K) to 10^4 ($T = 350$ K), at high frequency ($\nu = 10^6$ Hz) these differences are much smaller, from 14 ($T = 110$ K) to 100 ($T = 350$ K).

On the other hand, the imaginary part of the dielectric permittivity ε''_r shows rather high values, that increase almost linearly with temperature. As a result, this sample shows loss tangents ($\tan\alpha = \varepsilon''_r/\varepsilon'_r$) that also increase with temperature, with values ranging from 0.03 to 140.

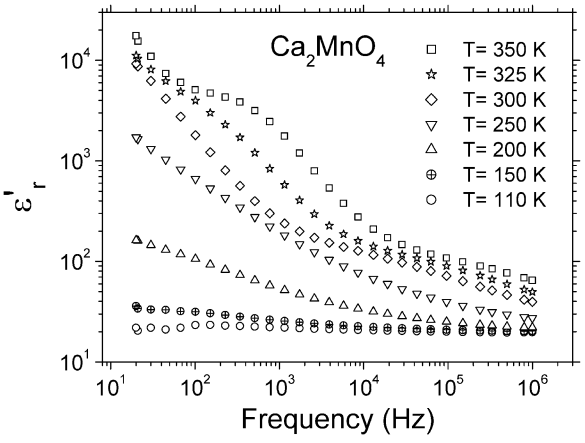

Fig. 2. Frequency dependence of the ε'_r values of the Ca_2MnO_4 sample at different temperatures.

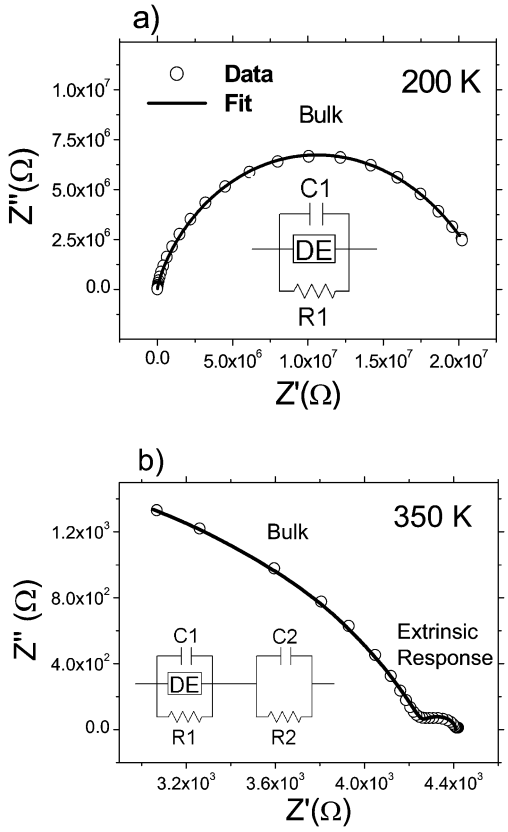

Fig. 3. Examples of the two kind of Z'' versus Z' diagrams found in the case of the Ca_2MnO_4 sample: a) Lower temperature region ($110 \leqslant T$ (K) < 300), showing basically the arc associated to the bulk response, b) higher temperature region ($300 \leqslant T$ (K) $\leqslant 350$), showing two arcs attributed to the bulk and extrinsic response. The solid line corresponds to the fit of the data to the equivalent circuits shown in the figures.

Typical impedance complex plane plots for this undoped sample are shown in Fig. 3: a) for the temperature interval $110 \leqslant T$ (K) < 300 and b) for $300 \leqslant T$ (K) $\leqslant 350$.

As it can be seen, in the range 110–300 K it shows a single large arc, while for $T \geqslant 300$ K a second small arc appears in the low frequency range.

The large arc can be modeled by an equivalent circuit containing three elements connected in parallel: a resistance (R) and a capacitance (C), that are frequency independent, and a frequency-dependent distributed element (DE). As this large arc intercepts zero (see Fig. 3a)), it seems to be associated with the material bulk response [24,26].

On the other hand, the second arc can be modeled as a single RC connected in series with the circuit that describes the bulk arc (Fig. 3b)). This small arc is associated to extrinsic contributions like grain boundaries or electrode effects.

According to these IS results, the low temperature region $T < 300$ K, where ε'_r presents lower values that are almost temperature independent in the high frequency region, the dielectric response of the materials is that of the bulk sample, that is, the dielectric behaviour is mainly intrinsic.

The intrinsic dielectric constant that can be calculated from the bulk capacitance obtained from the IS fit is ε'_r (bulk) $= 14$ (± 1).

Nevertheless, in the high temperature region, where ε'_r presents higher values and is strongly frequency dependent, the dielectric response is strongly affected by extrinsic factors (grain boundaries and electrode effects) related to Maxwell–Wagner polarization.

3.3.2. $Ca_{2-x}Pr_xMnO_4$ (charge-ordered compounds)

Fig. 4 shows the frequency dependence of the dielectric constant ε'_r for the Pr-doped samples.

As it can be observed, after an initial decrease at very low frequencies, related to diffusion processes that are not the aim of this work, the high dielectric constant keeps a constant value for a certain frequency range, and then decreases in a step-like manner as frequency gets higher. This behaviour is significantly different from what we find in the non-doped compound, where only a very small plateau is seen at the highest temperature and in the lowest frequency region.

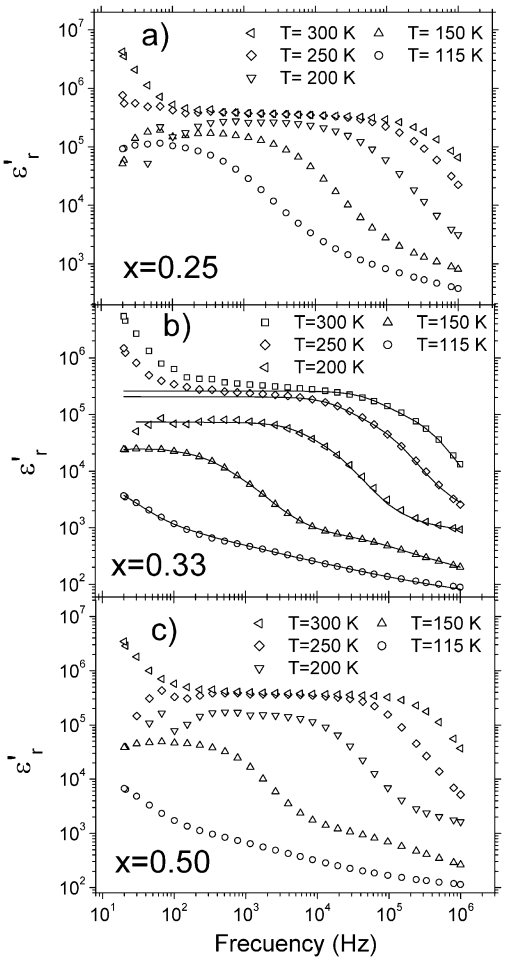

Fig. 4. ε'_r versus frequency for the Pr-doped samples $Ca_{2-x}Pr_xMnO_4$ with a) $x = 0.25$, b) $x = 0.33$ and c) $x = 0.50$. In the $x = 0.33$ sample, the solid line is the fit of the data to found in the case of the Pr-doped samples with $x = 0.33$ the equivalent circuits shown in Fig. 5.

The ε'_r values for these CO samples are very high ($\varepsilon'_r \approx 10^6$ in the plateau region) and about two orders of magnitude higher than those found in Ca_2MnO_4.

These results are nevertheless qualitatively similar to those reported in the literature for other compounds such as $CaCu_3Ti_4O_{12}$, $La_{2-x}Sr_xNiO_4$, $CaMn_7O_{12}$ etc. [12–14, 20,32].

The imaginary part of the dielectric permittivity ε''_r also shows high values, that increase with temperature, with loss tangents between 0.025 and 10^3.

In order to understand the dielectric behaviour of these CO Pr-doped compounds, IS analysis was also carried out. The impedance complex plane plot of the $x = 0.33$ sample, that are qualitatively similar to those of the $x = 0.25$ and $x = 0.50$, are shown in Fig. 5 for different temperature intervals. As it can be seen, at low temperatures ($T \leqslant 110$ K) it shows a single large arc that intercepts the origin; at intermediate temperatures ($120 \leqslant T$ (K) $\leqslant 200$) a second arc appears in the low frequency range; and at higher temperatures ($T > 200$ K) it shows an arc that does not intercepts the coordinates origin.

The impedance complex behaviour of these samples can be modeled by an equivalent circuit consisting of two parallel *RC* elements connected in series to a third element with a *R*, *C* and *DE* connected in parallel. As we will show later the two parallel *RC* elements simulate the extrinsic contribution (grain and electrodes boundaries) while the third element simulate the bulk contribution. This circuit is similar to the one used in the high temperature region of Ca_2MnO_4, but in the case of the Pr-doped samples a new *RC* is needed to fit the data attributed to extrinsic factors.

The number of elements in the equivalent circuit needed to simulate the impedance plane plots is different depending on the temperature.

At lowest $T \leqslant 110$ K, the impedance complex plane plot shows a large arc that can be modeled by a resistance, a capacitance and distributed element (*DE*), see Fig. 5a). As this large arc intercepts zero, it seems to be associated with the materials bulk response.

In the temperature range 110–200 K, the impedance complex plane plots show two arcs (see Fig. 5b)) that can be modeled by the equivalent circuit shown before. In Fig. 5b), we show as an example the fit at 170 K. The order of magnitude of the capacitance associated with the high frequency arc is about pF/cm, typical of bulk response [26], while the capacitance of the low frequency arc is about nF/cm, typical of extrinsic factors.

In the high temperature range ($T > 200$ K), the impedance complex plane plots show an arc which does not intercept the coordinates origin (Fig. 5c)), so this means that at these temperatures and in the frequency range studied only the response due to extrinsic factors is observed. This plot can be modeled with two *RC* elements connected in series and one *R*, in order to consider the resistance of the non-observed bulk. In this region, we do not have data to estimate the bulk capacitance, and we cannot obtain information about the intrinsic ε'_r (bulk) value at the charge ordering temperature. In fact, if we plot the measured ε'_r versus T (Fig. 6), the ε'_r value is mainly intrinsic at the lowest temperatures. But at higher temperatures $T > 150$ K, there is a notable rise of the permittivity probably due to the influence of extrinsic factors that does not allow us to obtain a clear information about the behaviour of the intrinsic dielectric response at the charge ordering temperature.

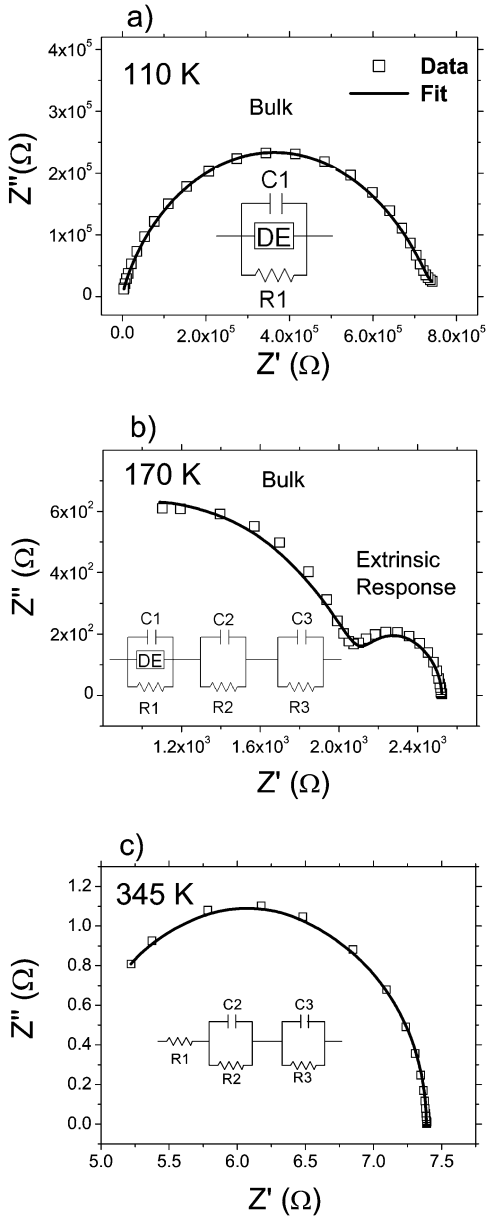

Fig. 5. Examples of the three kind of Z'' versus Z' diagrams found for the Pr-doped sample with $x = 0.33$ (a similar behavior was found in the case of the $x = 0.25$ and 0.50). a) Low temperature region ($T \leqslant 100$ K), showing basically the arcs associated to the bulk response, b) intermediate-temperature region ($120 \leqslant T$ (K) $\leqslant 200$), showing two arcs attributed to the bulk and extrinsic response, c) high temperature region ($T > 200$ K), where only the arc associated to the extrinsic contributions is observed.

The intrinsic dielectric constants calculated from the values of the obtained bulk capacitances were 217 (±30), 37

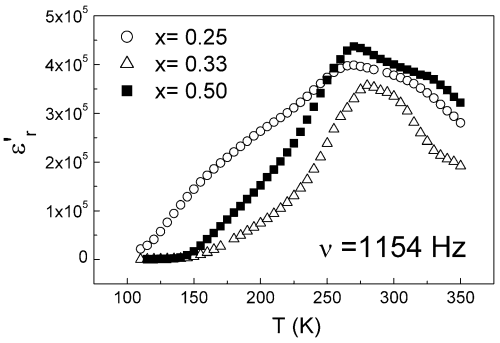

Fig. 6. Temperature dependence of the dielectric permittivity for Pr-doped samples, showing the dramatical increase of the ε'_r value as temperature increases (measuring frequency $\nu = 1154$ Hz).

(±3) and 80 (±4) for the $x = 0.25, 0.33$ and 0.50 samples, respectively. Taking into account that in these type of oxides ε'_r is typically of the order of 10 [23] the here-obtained values are remarkably high. If we compare them with the dielectric constant of the non CO compound $\varepsilon'_r(\text{bulk}) = 14$, these results suggest that the CO state may play an important role in these enhanced dielectric constants.

Specially large is the suspicious value of 217 obtained for the 0.25 sample. This value is notably higher than the value predicted for a non-ferroelectric material [25].

In order to confirm these results, the dielectric constants were also obtained graphically, see Fig. 7, by using the expression $\varepsilon'_r = \varepsilon'_r(\text{bulk}) + A\omega^{s-1}$ [15] (where $A = (\sigma_o/\varepsilon_o)\tan(s\pi/2)$, σ_o is generally weakly temperature dependent, ε_o is the permittivity of free space, s is the exponent of the power law and $\omega = 2\pi f$ is the angular frequency). These plots of ε'_r vs. ω^{s-1} at fixed temperatures yield $\varepsilon'_r(\text{bulk})$ as the common intercept (i.e., in the limit $\omega \to \infty$). At each temperature, s is determined from the frequency dependence of the conductivity $\sigma_{a.c.} = \sigma_{d.c.} + \sigma_o\omega^s$ (universal dielectric response [33]).

By this method, very similar values to those previously calculated for the dielectric constant of the Pr-compounds were obtained. In any case, for the $x = 0.25$ sample, the large $\varepsilon'_r(\text{bulk})$ value obtained, could indicate that extrinsic contributions might still be present even at the lowest measured temperature.

In addition to a high intrinsic dielectric constant, extrinsic effects enhance even further the dielectric response of these materials, specially at $T < 150$ K, and give rise to such very high room temperature dielectric constants ($\varepsilon'_r \sim 10^6$). More evidence for the influence of the extrinsic polarization effects in the dielectric measurements is given by performing the experiments with different kind of contacts [34]. In Fig. 8, we show the results obtained for the $x = 0.33$ sample at two different temperatures using sputtered gold, sputtered silver and silver paint contacts. As it can be seen, at 300 K the dielectric behaviour of the sample is different depending on the contacts used. In this case, the highest ε'_r values are obtained using sputtered silver and gold contacts, that lead to a larger area of direct metal-semiconductor contact; and

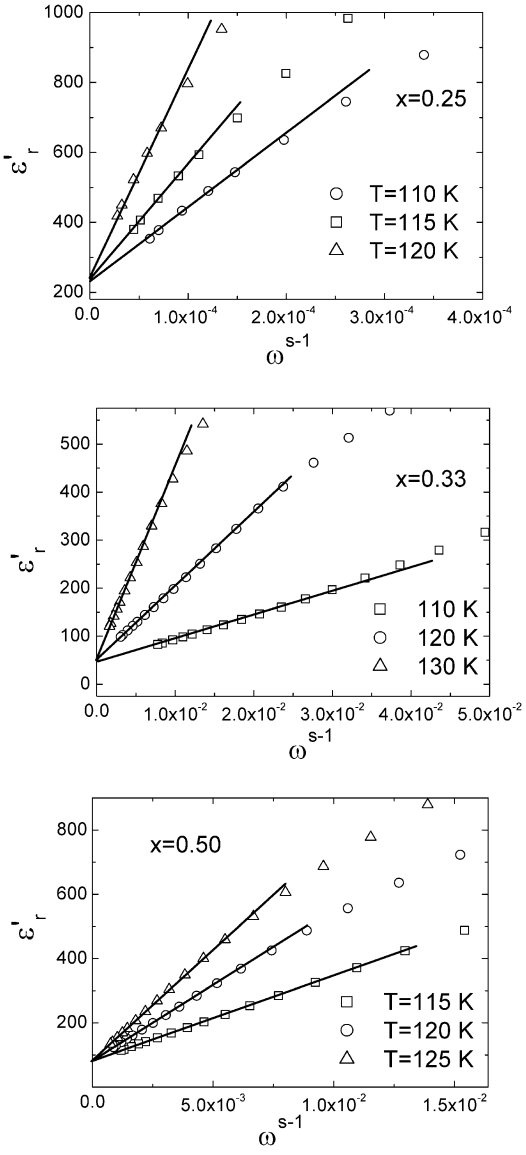

Fig. 7. ε'_r versus ω^{s-1} curves for the Pr-doped samples obtained at low temperatures ($T < 130$ K).

the lowest values using silver paint, due to the poorer area of contact of its relatively large particles. On the other hand, at low temperature (110 K) (where the behaviour is mainly due to the bulk material) the dielectric response is almost contact independent specially at high frequencies, confirming the non-interference of the electrodes.

4. Conclusions

$Ca_{2-x}Pr_xMnO_4$ ($x = 0, 0.25, 0.33$ and 0.50) samples were prepared by the Pechini method. Room temperature X-ray diffraction indicated that these compounds are single-phase and resistivity measurements on the Pr-doped samples showed evidences for CO transitions at 275, 330 and 315 K for $x = 0.25, 0.33$ and 0.50, respectively, and no CO for $x = 0$.

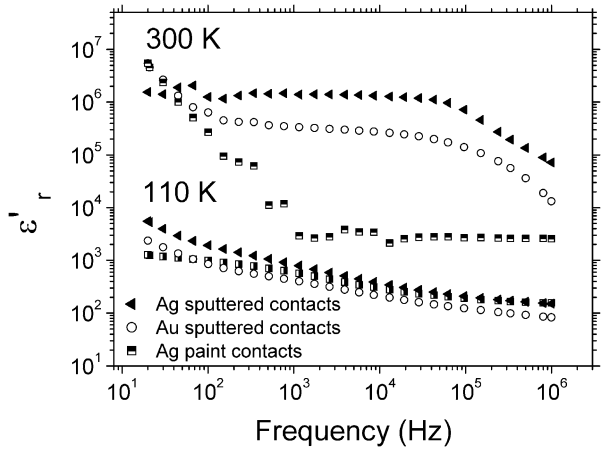

Fig. 8. Plot of ε'_r as a function of frequency for the $x = 0.33$ sample showing the influence of the type of contacts (sputtered gold, sputtered silver and silver paint) on the dielectric behaviour of this material (measuring temperatures: 110 and 300 K).

The intrinsic dielectric constants calculated by IS analysis from the values of the obtained bulk capacitances were 217, 37 and 80 for the $x = 0.25, 0.33$ and 0.50 samples, respectively. These values are remarkably large for oxide without off-center atoms that typically display ε'_r values of the order of 10. On the contrary, the non-charge-ordered compound Ca_2MnO_4 showed the expected value of 14. These results suggest that the CO state may play an important role in this increase of the dielectric constants. This opens a new direction to find materials with strong dielectric behaviour involving condensation of electronic charge.

The strong influence of extrinsic factors in the measured ε'_r values is also observed in the Pr-doped samples, enhancing even further their dielectric response and giving rise to such very high room temperature dielectric constants ($\varepsilon'_r \sim 10^6$).

Acknowledgements

We wish to acknowledge the financial support from DGICYT, Ministerio de Ciencia y Tecnología, Spain, under Project FEDER-MAT 2001-3749-C02-02.

References

[1] P. Shiffer, A.P. Ramirez, W. Bao, S.W. Cheong, Phys. Rev. Lett. 75 (1995) 3336.
[2] M. Imada, A. Fujimori, Y. Tokura, Rev. Mod. Phys. 70 (1998) 1039.
[3] Colossal magnetoresistance, in: C.N.R. Rao, B. Raveau (Eds.), Charge Ordering and Related Properties of Manganese Oxides, World Scientific, Singapore, 1998.
[4] E.J. Verwey, Nature 144 (1939) 327.
[5] R. Kajimoto, K. Ishizaka, H. Yoshizawa, Y. Tokura, Phys. Rev. B 67 (2003) 14511.
[6] S.A. Kivelson, I.P. Bindloss, E. Fradkin, V. Oganesyan, J.M. Tranquada, A. Kapitulnik, C. Howald, Rev. Mod. Phys. 75 (2003) 1201.
[7] H. Kuwahara, Y. Tomioka, A. Asamitsu, Y. Moritomo, Y. Tokura, Science 270 (1995) 961.
[8] Y. Moritomo, H. Kuwahara, Y. Tomioka, Y. Tokura, Phys. Rev. B 55 (1997) 7549.
[9] C. Jardón, F. Rivadulla, L.E. Hueso, A. Fondado, J. Rivas, M.A. López Quintela, R. Zysler, M.T. Causa, P. Sande, J. Magn. Magn. Mater. 196–197 (1999) 475.
[10] F. Rivadulla, M.A. López Quintela, L.E. Hueso, C. Jardón, A. Fondado, J. Rivas, M.T. Causa, R.D. Sánchez, Solid State Commun. 110 (1999) 179.
[11] J. Sichelschmidt, M. Paraskevopoulos, M. Brando, R. Wehn, D. Ivannikov, F. Mayr, K. Pucher, J. Hemberger, A. Pimenov, H.-A. Krug von Nidda, P. Lunkenheimer, V.Y. Ivanov, A.A. Mukhin, A.M. Balbashov, A. Loidl, Eur. Phys. J. B 20 (2001) 7.
[12] J. Rivas, B. Rivas-Murias, A. Fondado, J. Mira, M.A. Señarís Rodríguez, Appl. Phys. Lett. 85 (2004) 6224.
[13] S. Yáñez Vilar, A. Castro-Couceiro, B. Rivas-Murias, A. Fondado, J. Mira, J. Rivas, M.A. Señarís-Rodríguez, Zeitschrift für Anorganische und Allgemeine Chemie, in press.
[14] A. Castro-Couceiro, S. Yáñez Vilar, B. Rivas-Murias, A. Fondado, J. Mira, J. Rivas, M.A. Señarís-Rodríguez, J. Appl. Phys., 2004, in press.
[15] J.L. Cohn, M. Peterca, J.J. Neumeier, Phys. Rev. B 70 (2004) 214433.
[16] J.L. Cohn, M. Peterca, J.J. Neumeier, J. Appl. Phys. 97 (2005) 034102.
[17] G.H. Jonker, J.H. van Santen, Science 109 (1949) 632.
[18] D.V. Efremov, J. Van den Brink, D.I. Khomskii, Nature Mater. 3 (2004) 853.
[19] R.J. Cava, J. Mater. Chem. 11 (2001) 54.
[20] M.A. Subramanian, D. Li, N. Duan, B.A. Reisner, A.W. Sheight, J. Solid State Chem. 151 (2000) 323.
[21] M. Ibarra, R. Retoux, M. Hervieu, C. Autret, A. Maignan, C. Martin, B. Raveau, J. Solid State Chem. 170 (2003) 361.
[22] C.J. Maxwell, Electricity and Magnetism, Clarendon Press, Oxford, 1982.
[23] A. Von Hippel, Dielectric and Waves, Artech House, Boston, London, 1995.
[24] D.C. Sinclair, T.B. Adams, F.D. Morrison, A.R. West, Appl. Phys. Lett. 80 (2002) 2153.
[25] P. Lunkenheimer, V. Bobnar, A.V. Pronin, A.I. Ritus, A. Volkov, A. Loidl, Phys. Rev. B 66 (2002) 52105.
[26] J. Ross MacDonald, Impedance Spectroscopy Emphasizing Solid Materials and Systems, Jonh Wiley & Sons, NewYork, 1987.
[27] F. Licci, T. Besagni, L. Rinaldi, European Patent Appl. No. 85860253-2 (1985).
[28] C.J. Howard, H. Hunter, Rietica: A computer program for Rietveld analysis of X-ray and neutron powder diffraction patterns, Australian Nuclear Science and Technology Organization Lucas Heights Research Laboratories.
[29] H. Takashima, R. Wang, N. Kasai, A. Shoji, Appl. Phys. Lett. 83 (2003) 2883.
[30] J. Ross Macdonald, LEVM version 8.0, Complex nonlinear squares fitting program, 2003.
[31] M.E. Leonowicz, K.R. Poeippelmeier, J.M. Longo, J. Solid State Chem. 59 (1985) 71.
[32] C.C. Homes, T. Vogt, S.M. Shapiro, S. Wakimoto, A.P. Ramirez, Science 293 (2001) 673.
[33] A.K. Jonscher, Dielectric Relaxation in Solids, Chelsea Dielectric Press, London, 1983.
[34] P. Lunkenheimer, R. Fichtl, S.G. Ebbinhaus, A. Lloidl, Phys. Rev. B 70 (2004) 172102.